2010 11th Int. Conf. Control, Automation, Robotics and Vision
Singapore, 7-10th December 2010

Trajectory Generation of Straightened Knee Walking for Humanoid Robot iCub

Zhibin Li, Nikos G. Tsagarikis, Darwin G. Caldwell
Department of Advanced Robotics
Italian Institute of Technology
Genova, Italy
zhibin.li@iit.it, nikos.tsagarakis@iit.it, darwin.caldwell@iit.it

Bram Vanderborght
Department of Mechanical Engineering
Vrije Universiteit Brussel
Brussels, Belgium
bram.vanderborght@vub.ac.be

***Abstract*—Most humanoid robots walk with bent knees, which particularly requires high motor torques at knees and gives an unnatural walking manner. It is therefore essential to design a control method that produces a motion which is more energy efficient and natural comparable to those performed by humans. In this paper, we address this issue by modeling the virtual spring-damper based on the cart-table model. This strategy utilizes the preview control, which generates the desired horizontal motion of the center of mass (COM), and the virtual spring-damper for generating the vertical COM motion. The theoretical feasibility of this hybrid strategy is demonstrated in Matlab simulation of a multi-body bipedal model. Knee joint patterns, ground reaction force (GRF) patterns, COM trajectories are presented. The successful walking gaits of the child humanoid "iCub" in the dynamic simulator validate the proposed scheme. The joint torques required by the proposed strategy are reduced, compared with the one required by the cart-table model.**

***Index Terms*—trajectory generation, straightened knee walking, bipedal walking**

I. Introduction

Humanoids are now able to perform a variety of stable walking gaits [1], [2], [3], [4]. This has been addressed using a variety of techniques based on simplified models. The multi-dimensional control problem can be simplified by controlling the center of mass (COM), which highly represents the translational dynamics. Furthermore, a constant COM height turns the non-linear spatial COM motion into a linear form, known as the cart-table model [5]. However, the invariant COM height in turn leads to the knee singularities occurring at times. These singularities are typically addressed by walking with bent knees which keeps a low COM height. Nevertheless, the joint motors need to counteract the gravitational torque. Particularly, the knee motors usually have the highest torque demand and power consumption [3]. In contrast, in human walking, the knee is almost completely stretched [6] and performs mostly negative work [7]. Hence, we are motivated to study a new control method which permits humanoid walking with more straightened knees to minimize energy consumption at joint motors.

WABIAN-2 [8] achieved a more straightened knee walking without knee singularities by using the predetermined knee joint trajectories consisting of two sinusoidal motions. This walking style claims to be more human-like due to the more straightening knees. Moreover, it brings an important benefit in terms of less torque and energy requirement than conventional walking with bent knees [8], [9]. However, it needs two extra degree of freedoms (DOF) at waist joint for solving inverse kinematics. Handharu et al. [10] designed a hip trajectory satisfying ZMP by the method in [11], and solved the inverse kinematics by defining an initial foot trajectories. The knee stretch motions are obtained by cubic spline interpolation to prevent singularities. Accordingly, the foot trajectories need to be redesigned to find the inverse kinematics solution to satisfy the new knee trajectories. In short, both of these two methods plan knee motion in the joint space.

As a simple approximation, an inverted pendulum [12] model is often used to represent human walking, and a more complex spring-mass model is used to simulate human running [13]. Lately, Geyer [14] showed that the compliant rather than the stiff legs are essential to obtain the basic walking mechanics, such as ground reaction force (GRF) pattern, and introduced a spring-mass model for walking as well as running. In this paper, inspired by Geyer's study of the compliant legs, we incorporate the virtual spring-damper model into the conventional cart-table model to obtain a more straightened knee walking which is more energy efficient and more comparable to humans. Our method plans a walking pattern in the Cartesian space without predefining or redesigning the knee joint trajectories.

This paper is organized as follows. Section II presents the fundamentals of the preview control, examines the compatibility issue, and formulates the virtual spring-damper model. Section III applies the new scheme to generate the stable gait of straightened knee walking, revealing knee joint, GRF, and COM patterns. In section IV, the dynamic simulation in OpenHRP3 [15] shows the decreasing joint torques in the straightened knee walking compared with that required by the conventional method.

II. Mathematical Modeling

In this study, we use the cart-table model to generate horizontal motion, and the virtual spring damper model to produce vertical motion. Considering that the x and y motion is solved by the preview control, we focus on the generation of vertical motion in order to achieve the straightened knee walking.

A. Preview Control Scheme

Kajita et al. [5] proposed a cart-table model which assumes a simplified robot model where a running cart of mass m is placed on a pedestal mass-less table. If the COM of a cart at rest is outside of the foot area of the table, the table will fall. However, the zero moment point (ZMP) [16] can be positioned inside the support polygon by choosing a proper horizontal acceleration. The advantage of this method is that it generates a desired horizontal motion of the COM given the various footholds or arbitrary ZMP trajectories. A dynamic system described by the state space equations is available if the jerk $u_x = d\ddot{x}/dt$ is defined. Thus, by applying the state space equations, walking pattern generation can be treated as a servo tracking problem. This generator outputs a COM trajectory which results in a ZMP trajectory that tracks the reference one. An optimal control strategy [17] is used to resolve this tracking problem by synthesizing future information. It is therefore also called preview control since it takes future reference into account. In this study, the preview time window is 2 s.

The cart-table model is a single mass simplification of a real robot, thus the deviations between a single mass model and the real robot exists. A stable walking pattern for cart-table model may exhibit instability for a real robot. Therefore, a second stage of preview control compares the reference ZMP and the one computed from a multi-body model in order to further minimize the ZMP tracking errors.

B. Compatibility

Prior to applying the virtual model, we mathematically examine the feasibility of combining the cart-table model and the virtual model. The cart-table model assumes that the cart stays on a flat table, while the virtual spring is meant to create vertical displacement. Introducing the virtual spring-damper seems to theoretically violate the assumption of the cart-table model. However, the following analysis shows that the error would be insignificant if the vertical acceleration is relatively small compared to the gravitational acceleration.

A general ZMP equation omitting the rate of angular momentum is

$$x_{zmp} = x - \frac{\ddot{x}z}{\ddot{z}+g} \tag{1}$$

The simplified ZMP equation of cart-table model used by the preview controller is

$$x'_{zmp} = x - \frac{\ddot{x}z_c}{g} \tag{2}$$

, where z_c is the constant COM height.

The ZMP error introduced by the vertical motion is

$$e_x = x_{zmp} - x'_{zmp} = \ddot{x}\frac{z_c\ddot{z} + g(z_c - z)}{g(\ddot{z}+g)} \tag{3}$$

Partial differential equations of ZMP error e_x are

$$\frac{\partial(e_x)}{\partial(z)} = -\frac{\ddot{x}}{\ddot{z}+g} \tag{4}$$

$$\frac{\partial(e_x)}{\partial(\ddot{z})} = \ddot{x}\left(\frac{z_c}{g(\ddot{z}+g)} - \frac{(z_c\ddot{z} + gz_c - gz)}{g(\ddot{z}+g)^2}\right) \tag{5}$$

Linearize the partial derivatives around the equilibrium condition z_c and $\ddot{z} = 0m/s^2$, the ratio of error caused by $\Delta\ddot{z}$ and Δz are

$$\left|\frac{\partial(e_x)}{\partial(\ddot{z})}\Delta\ddot{z}\right| / \left|\frac{\partial(e_x)}{\partial(z)}\Delta z\right| = \left|-z/(\ddot{z}+g)\right| \left|\Delta\ddot{z}/\Delta z\right| = \frac{\left|\Delta\ddot{z}/g\right|}{\left|\Delta z/z_c\right|} \tag{6}$$

In bipedal walking, assume $z_c \approx 1m$ for the adult human-size robot, $|\Delta z| \leq 0.02m$, $|\Delta\ddot{z}| \leq 2m/s^2$. Substituting these values into (6), we gain the insight that the height variation $\Delta z/z_c$ is relatively small compared with the acceleration variation $\Delta\ddot{z}/g$. So, e_x introduced by vertical COM motion is mainly determined by $\Delta\ddot{z}$. Therefore, e_x can be reduced by minimizing the acceleration term $\Delta\ddot{z}/g$ within a certain bound.

C. Virtual Spring-damper Model

On the basis of the cart-table model, the virtual spring-damper model relaxes the constraint of constant COM height. This will permit greater stretching of knee joints which will reduce the knee torque and provide a more natural motion.

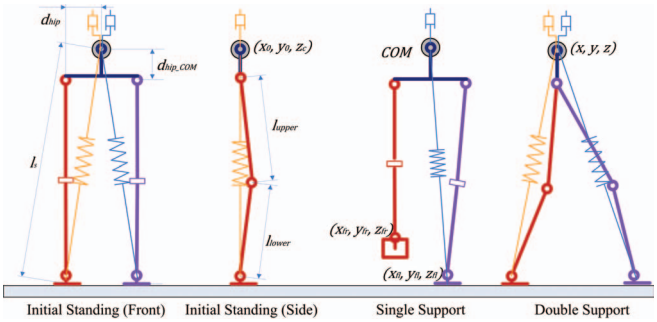

Fig. 1. Virtual spring-damper model

In Fig. 1, the virtual springs connect the COM and the ankle joints. During walking, the virtual springs are compressed thus generating virtual forces. Since preview control solves the horizontal motion, only the vertical force component of the spring is employed to determine the vertical dynamics. In z axis, a virtual damper is added at each spring tip to prevent vertical oscillations. The parameters are listed below.

l_{s_l}, l_{s_r}:the spring length for the left and right leg support respectively;
l_0: the original rest length of the spring;
l'_0: the original rest length of the spring;
l_{upper}: the length of the upper leg;
l_{lower}: the length of the lower leg;
d_{hip}: the distance from the hip joint to the hip center;
$d_{hip_{COM}}$: the initial distance between the hip center and COM;
x,y,z: the positions of COM in the global coordinate;
x_{fl},y_{fl},z_{fl}, x_{fr},y_{fr},z_{fr}: the positions of the left and right foot in the global coordinate;
K: the mass-less stiffness k/m of the virtual spring;
C: the mass-less viscous coefficient c/m of the virtual damper;
g: the gravitational constant $9.81m/s^2$.

We define the mass-less coefficient K and C, thus system dynamics is preserved regardless of a specific mass m of

the robot. Tuning K and C is intuitive due to their physical meanings.

We have studied smooth transition strategies to minimize $\Delta\ddot{z}$ in order to compensate for the overall ZMP error in the 2nd preview control.

1) *Transition from initial standing to single support phase*: halve the stiffness of each leg in standing phase.
2) *Transitions from single support phase to double support phase*: set the initial spring length in the event of touch-down as its temporary rest length l_0', ensuring the vertical acceleration exerted by the touch-down leg increases from zero.
3) *Transitions from double support phase to single support phase*: restore the original spring rest length l_0, and the small force spikes caused by this stiffness change will be absorbed by the virtual damper.

The simulated robot at the initial standing phase has massless stiffness of $0.5K$ at each leg. So the equivalent stiffness of two legs is K. When the robot starts the first single support phase, its support leg also has the same stiffness of K, so $\ddot{z}$ doesn't change dramatically. When the robot enters the double support phase, the touch-down leg doesn't fully straighten for avoiding the singularity. So, at the very beginning of the touch-down, the virtual spring length l_s is already shorter than its rest length l_0. Consequently, a non-zero initial force is generated and contributes an offset force input which results in a large acceleration $\ddot{z}$. To avoid this, the virtual spring length l_s in the event of the touch-down is set as its temporary rest length, denoted as l_0', to ensure that the $\ddot{z}$ exerted by the touch-down leg increases from zero. This realizes smooth transitions of the vertical acceleration.

With the above smooth transition strategies, Δz and $\Delta\ddot{z}$ can be treated as small parametric disturbances which can be compensated by the 2nd loop of the preview controller.

In the single support phase,

$$\ddot{z} = K(l_0/l_s - 1)z - g - C\dot{z} \tag{7}$$

,where l_0 is

$$l_0 = \sqrt{(l_{upper} + l_{lower} + d_{hip_{COM}})^2 + d_{hip}^2} \tag{8}$$

, and l_s is

$$l_{s_l} = \sqrt{(x - x_{fl})^2 + (y - y_{fl})^2 + z^2} \tag{9}$$

$$l_{s_r} = \sqrt{(x - x_{fr})^2 + (y - y_{fr})^2 + z^2} \tag{10}$$

, for the left and right support leg respectively.

In the double support phase, the dynamic equation is

$$\ddot{z} = K(l_0/l_{s_{old}} + l_0'/l_{s_{new}} - 2)z - g - 2C\dot{z} \tag{11}$$

, where l_0' is the temporary rest spring length of the latest touch-down leg $l_{s_{new}}$. (Either $l_{s_{new}} = l_{s_l}$, $l_{s_{old}} = l_{s_r}$ or $l_{s_{new}} = l_{s_r}$, $l_{s_{old}} = l_{s_l}$).

In the initial standing position, denote COM as (x_0, y_0, z_c), where $x_0 = 0, y_0 = 0$, we have

$$(\frac{2l_0}{\sqrt{d_{hip}^2 + z_c^2}} - 2)z_c = \frac{g}{K} \tag{12}$$

Rewrite (12), yields

$$z^4 + \frac{g}{K}z^3 + (\frac{g^2}{4K^2} + d_{hip}^2 - l_0^2)z^2 + \frac{gd_{hip}^2}{K}z + \frac{g^2 d_{hip}^2}{4K^2} = 0 \tag{13}$$

Solve (13) to obtain z_c as the constant COM height in the state space equation of the preview controller. Given the initial condition $z(0) = z_c, \dot{z}(0) = 0, \ddot{z}(0) = 0$, the COM state $(z(i), \dot{z}(i), \ddot{z}(i))$ can be computed by numerical integrations according to (7) to (11).

D. Flow Chart of Control Algorithms

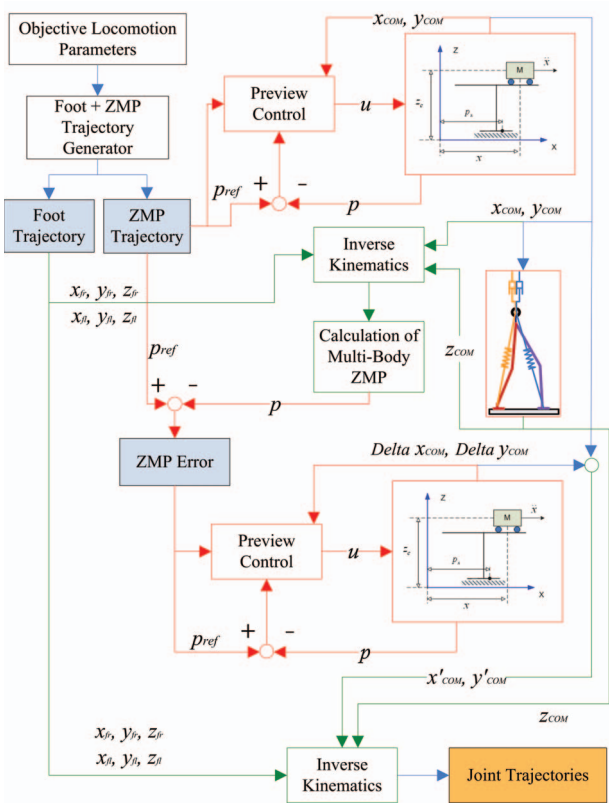

Fig. 2. Flow chart of overall scheme

Simulation algorithms are summarized in Fig. 2. The virtual spring model is integrated into the preview control scheme based on the formulas and strategies proposed above. The compatibility is established on the premises that the errors yielded by Δz and $\Delta\ddot{z}$ are constrained within certain range by implementing smooth transition strategies. Therefore, we only incorporate the virtual spring-damper model into the first preview control loop to obtain a height varying hip pattern. In the second control loop, the preview control modulates the hip motion only in x and y axes for compensating ZMP errors.

III. Trajectory Generation of Straightened Knee Walking

A. Simulation of Stable Walking Gait

We use the control scheme presented in Fig. 2 for the control of a simulated 12 DoF bipedal robot. The simulated robot represents the child humanoid robot iCub, which is a small robot with hip height less than 0.5 m so that it can't take a very large step. The robot model is built according to iCub's physical parameters, and more technical details are available in [18]. The simulated robot has distributed masses made of up seven rigid segments, namely each thigh, calf, foot, and the pelvis and the upper body as a whole. For each segment, the mass and the inertia tensor around its COM are used to represent the rigid body property. In this scenario, locomotion parameters are as follows.

1) *Step length*: $L_s = 0.15m$;
2) *Step Height*: $H_s = 0.02m$;
3) *Walking Cycle*: $T_c = 1s$;
4) *Number of simulated steps*: 6

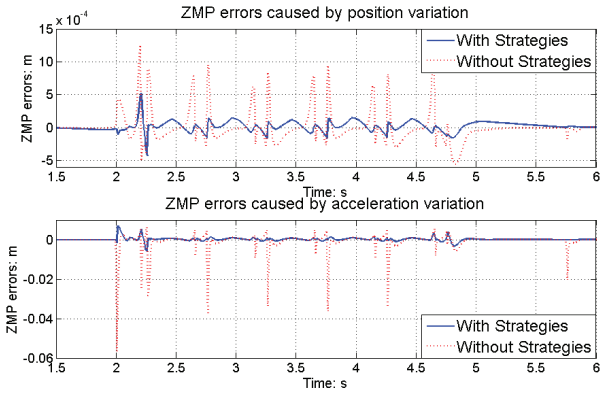

Fig. 3. ZMP errors caused by z and $\ddot{z}$ variation

The ZMP error e_x is calculated by (3) in order to investigate the assumption discussed in section II-B. Fig. 3 shows the first error term $(z_c - z)\frac{\ddot{x}}{\ddot{z}+g}$ caused by the height variation, and the second error term $z_c\frac{\ddot{x}\ddot{z}}{g(\ddot{z}+g)}$ caused by acceleration variation, respectively. The red dotted line is the ZMP error without smooth transition strategies, while the blue solid line is the one with the strategies applied. The simulation confirms that acceleration variation $\Delta\ddot{z}$ dominates the overall error e_x. Even without smooth transition strategies, the error caused by Δz is within 1 cm. However, the second term caused by $\Delta\ddot{z}$ increases up to 6 cm. In this scenario, the smooth transition strategies minimize overall error e_x within 7 mm. It proves that the cart-table model still highly represents the dynamics of a robot even with certain vertical motion.

Fig. 4 illustrates the ZMP tracking performance. The blue trace shows the desired ZMP trajectory, while the red line is the ZMP computed from the multi-body model after the $2nd$ preview control stage. The COM motion is in black line. The ZMP trajectory has minor tracking errors so the ZMP always remains in the support polygon. Hence, the ZMP criterion

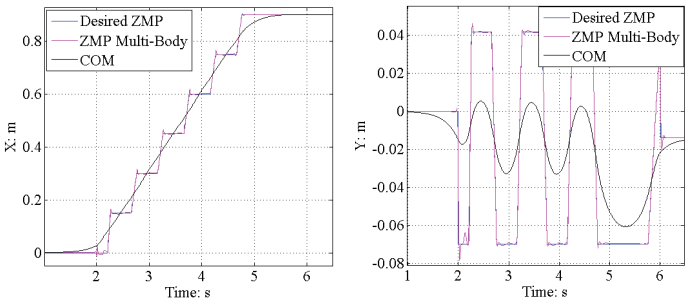

(a) x_{zmp} and COM trajectory (b) y_{zmp} and COM trajectory

Fig. 4. Simulated ZMP and COM trajectories

is met [16], which indicates a stable walking gait. It also confirms the concept of treating bounded height variation as a disturbance, which can be further minimized by the second preview control stage.

B. Knee Joint Patterns

The work in [7] shows that the statistical maximum knee angle during the stance phase is approximately 23^o for humans, while Fig. 5 shows that the simulated robot has around 26^o in general. When the robot places a touch-down leg, the knee joint angle increases due to the compression of the virtual spring, and decreases because of the decompression of the virtual spring. This leads to a convex knee joint pattern during the robot's stance phase, shown in Fig. 5. The similar convex curve of knee joint is also revealed in human gait [7].

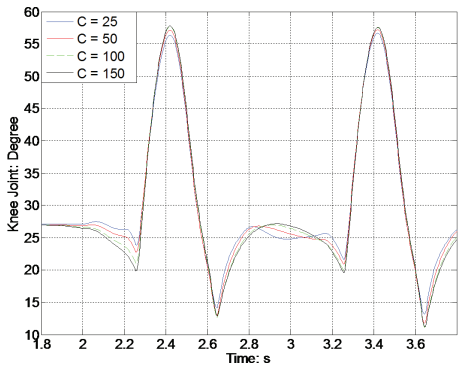

Fig. 5. Knee joint pattern with different C

A low value of mass-less viscous coefficient C causes larger vertical COM oscillations which results in double peaks in the knee angle during the stance phase. Tuning C resolves this issue. Hereby, C is assigned $25s^{-1}$, $50s^{-1}$, $100s^{-1}$, and $150s^{-1}$ respectively to demonstrate its influence on straightened knee walking.

C. GRF Patterns

As analyzed in section III-B, the virtual spring has the double compressions during the stance phase. Therefore, it consequently creates a double force peaks. This phenomenon is also observed in the study of biomechanical research of human

gait [7]. In Fig. 6, the normalized GRF of the human gait and the simulated robot are depicted. There are four similar features which reflect the similarities, despite that the GRF of the simulated robot has a smaller amplitude than that of humans.

1) *Double force peaks during single support phases*. Both the human and the robot show two force peaks larger than the body weight.
2) *Maximum force peak in double support phase*. Robot's touch-down leg produces additional force compared to single support case, thus the overlapping of two M shape forces results in a maximum force peak.
3) *The first force peak is larger than the second one in single support phase*. The viscous force F_v dissipates partial COM kinetic energy. As a result, the second force peak has smaller magnitude than the first one.
4) *Between the double peaks, both GRF patterns decreases in a sharper slope and subsequently increases relatively slower before reaching the second force peak*. According to virtual spring-damper model, the viscous property plays an importance role in this GRF pattern. Energy loss causes the mean velocity in posterior phase to be slower than that of the anterior phase. So in the anterior phase, the viscous force F_v is more significant, and meanwhile acts at the same direction as gravity mg to counteract the spring force F_s, which results in a remarkable decrease in the GRF pattern.

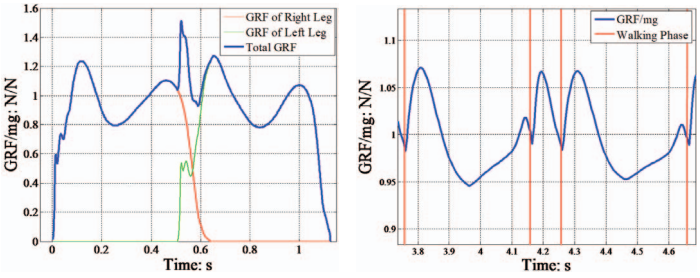

(a) GRF of humans (b) GRF of simulated robot

Fig. 6. GRF comparison of human and robot

To a certain extent, the integration of the virtual spring-damper and the cart-table model resembles the GRF pattern of human gait, although the fundamental principles are different. The human body contains tendons and ligaments which have compliant property. In contrast, the robot, a mechatronic system, has no such feature. The likeness is basically due to the modeling of the virtual elements, such as springs and dampers. Hence, the likeness depends on the K and C parameters.

D. COM Trajectory

Fig. 7 shows a spatial COM trajectory. It can be observed that the COM reaches maximum lateral displacement and maximum vertical position simultaneously. The algorithm exploits the dynamics of the virtual spring-damper models, in order to obtain a variable hip height. Both K and C have physical interpretations which are intuitively related to dynamic behaviors.

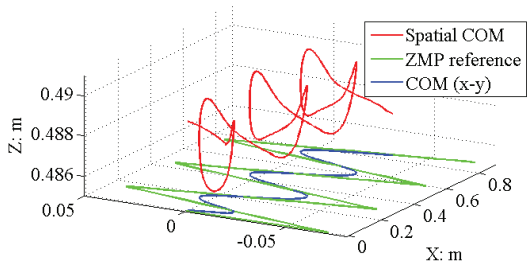

Fig. 7. Spatial COM trajectory

This spatial COM trajectory depends on its dynamics instead of being predefined. Therefore, the COM trajectory would vary from step to step given different footholds allocation or K and C values.

IV. Dynamic Simulations

In order to validate the effectiveness of the proposed method, we perform the dynamic simulations to examine the walking performance. The dynamic simulator OpenHRP3 [15] is used. The mass and inertia tensor configuration of the model are identical to iCub parameters [18]. The joint angles and velocities are the reference inputs for the joint controllers. All the joint motors use PID tracking control to execute the references.

A. Conventional and Straightened Knee Walking

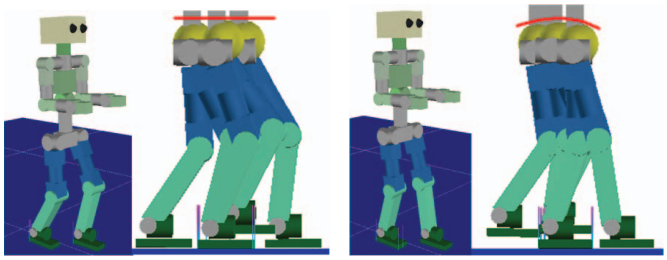

(a) Bent knee walking (b) Straightened knee walking

Fig. 8. Simulation of conventional bent knee walking and straightened knee walking

Fig. 8 shows both the conventional and straightened knee walking in the dynamic simulation. The yellow spherical ball represents the overall COM. The snapshots are three successive walking motions spaced at 0.2 s apart. Fig. 8(a) displays the conventional walking with bent knees, which is commonly seen in the humanoids walking, and the constant hip height feature is marked by the red straight line. Fig. 8(b) illustrates the straightened waking, and the variable hip height is highlighted by a wavy red curve.

In this study, we claim that a more natural manner of walking is in terms of more straightened knees and the convex keen joint patterns. The proposed method allows the robot to walk with more straightened knees compared with the results of conventional cart-table method, shown in Fig. 8. With the new scheme applied, the robot places its front foot with a

almost straight leg, and the stance leg is meanwhile more straightening rather than highly bent. The walking manner is more natural looking because humans also stretch out the front leg for the heel-contact [7].

B. Evaluation of Energy Efficiency

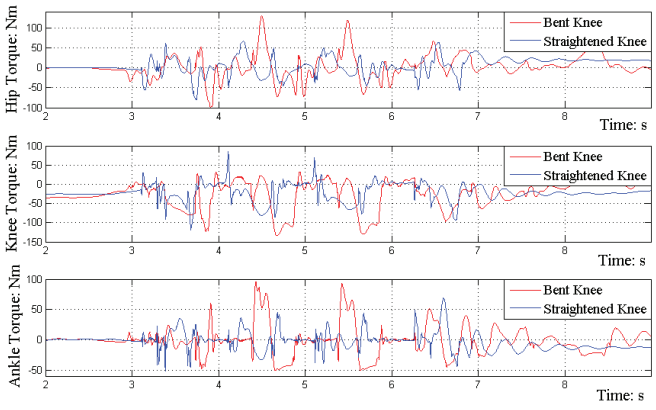

Fig. 9. Torques of the sagittal joints

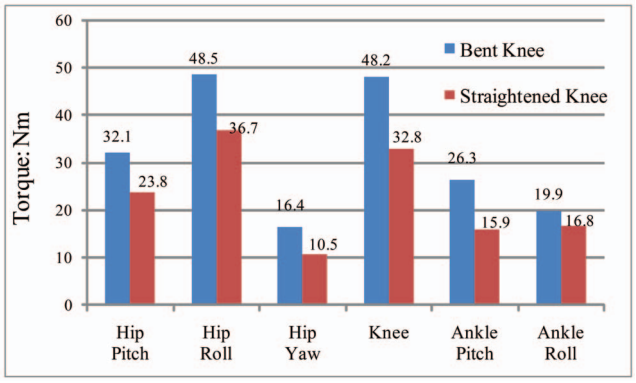

Fig. 10. Root mean square of all joint torques

Fig. 9 shows the sagittal joint torques. Compared to the bent knee walking, the straightened knee walking has smaller torque peaks, especially at stance phase. The electric power consumption is measured in terms of motor current, which is proportional to the motor torque. Therefore, the root mean square (RMS) torque (T_{RMS}) is an index to evaluate the energy efficiency. The T_{RMS} of all the joints are computed based on the original torque data obtained in the dynamic simulation, demonstrated in Fig. 10. The proposed method significantly reduces the power consumption at all joints. The The total RMS torque of all joints decreases from 191.4 Nm (bent knee) to 136.5 Nm (straightened knee), requiring 28.7% less.

V. Conclusion

The combination of the preview control and the virtual spring-damper model generates walking patterns which are more comparable to humans in terms of almost straightened knee joints. Additionally, the interesting features of the knee joint angle, GRF pattern, and the COM trajectory are also revealed. The dynamic simulation confirms the energy efficiency of the straightened knee walking.

Acknowledgment

This work is supported by the FP7 European project AMARSi (ICT-248311). The authors also sincerely thanks Jean-Christophe PALYART LAMARCHE for the force plate data of the human gait study.

References

[1] T. Matsui, H. Hirukawa, Y. Ishikawa, N. Yamasaki, S. Kagami, F. Kanehiro, H. Saito, and T. Inamura, "Distributed real-time processing for humanoid robots," in *IEEE International Conference on Embedded and Real-Time Computing Systems and Applications (RTCSA 2005)*, pp. 205–210, August 2005.

[2] P. Ill-Woo, K. Jung-Yup, L. Jungho, and O. Jun-Ho, "Online free walking trajectory generation for biped humanoid robot KHR-3(HUBO)," in *IEEE International Conference on Robotics and Automation (ICRA 2006)*, pp. 1231–1236, May 2006.

[3] Y. Ogura, H. Aikawa, H. ok Lim, and A. Takanishi, "Development of a human-like walking robot having two 7-dof legs and a 2-dof waist," in *ICRA*, pp. 134–139, 2004.

[4] Z. Peng, Q. Huang, X. Zhao, T. Xiao, and K. Li, "Online trajectory generation based on off-line trajectory for biped humanoid," in *IEEE International Conference on Robotics and Biomimetics (ROBIO 2004)*, pp. 752– 756, Augustus 2004.

[5] S. Kajita, F. Kanehiro, K. Kaneko, K. Fujiwara, K. Harada, K. Yokoi, and H. Hirukawa, "Biped walking pattern generation by using preview control of zero-moment point," in *IEEE International Conference on Robotics and Automation (ICRA 2003)*, vol. 2, pp. 1620–1626, May 2003.

[6] R. M. Alexander, *Exploring Biomechanics: Animals in Motion*. Scientific American Library, 1992.

[7] D. Winter, "Biomechanics and motor control of human movement," 1990.

[8] Y. Ogura, Hun-ok Lim, and A. Takanishi, "Stretch walking pattern generation for a biped humanoid robot," in *IEEE/RSJ International Conference on Intelligent Robots and Systems (IROS 2003)*, vol. 1, pp. 352–357, October 2003.

[9] Y. Ogura, T. Kataoka, H. Aikawa, K. Shimomura, Hun-ok Lim, and A. Takanishi, "Evaluation of various walking patterns of biped humanoid robot," in *IEEE International Conference on Robotics and Automation (ICRA 2005)*, pp. 603–608, April 2005.

[10] N. Handharu, J. Yoon, and G. Kim, "Gait pattern generation with knee stretch motion for biped robot using toe and heel joints," in *International Conference on Humanoid Robots, Daejeon, Korea*, pp. 265 – 270, 2008.

[11] Q. Huang, K. Yokoi, S. Kajita, K. Kaneko, H. Arai, N. Koyachi, and K. Tanie, "Planning walking patterns for a biped robot," *IEEE Transactions on Robotics and Automation*, vol. 17, pp. 280–289, June 2001.

[12] S. Mochon and T. McMahon, "Ballistic walking," *Journal of Biomechanics*, vol. 13, pp. 49–57, 1980.

[13] R. Blickhan, "The spring-mass model for running and hopping," *Journal of Biomechanics*, vol. 22, pp. 1217–1227, 1989.

[14] H. Geyer, A. Seyfarth, and R. Blickhan, "Compliant leg behaviour explains basic dynamics of walking and running," *Proceedings of the Royal Society B: Biological Sciences*, vol. 273, no. 1603, p. 2861, 2006.

[15] F. Kanehiro, H. Hirukawa, and S. Kajita, "OpenHRP: Open architecture humanoid robotics platform," *The International Journal of Robotics Research*, vol. 23, no. 2, pp. 155–165, 2004.

[16] M. Vukobratovic and B. Borovac, "Zero-moment point - thirthy five years of its life," *International Journal of Humanoid Robotics*, vol. 1, pp. 157–173, 2004.

[17] T. Katayama, T. Ohki, T. Inoue, and T. Kato, "Design of an optimal controller for a discrete time system subject to previewable demand," in *Int. J. Control*, vol. 41, pp. 677–699, 1985.

[18] N. Tsagarakis, G. Metta, G. Sandini, D. Vernon, R. Beira, F. Becchi, L. Righetti, J. Santos-Victor, A. Ijspeert, M. Carrozza, *et al.*, "iCub: the design and realization of an open humanoid platform for cognitive and neuroscience research," *Advanced Robotics*, vol. 21, no. 10, pp. 1151–1175, 2007.